DALTON
FULL PAPER

A new $Fe^{III}(\mu\text{-}OCH_3)_2(\mu\text{-}OAc)Fe^{III}$ complex containing phenolate and imidazole ligands as a structural model for the active site of non-heme diiron enzymes †

Marciela Scarpellini,[a] Ademir Neves,*[a] Adailton João Bortoluzzi,[a] Ivo Vencato,[a] Valderes Drago,[b] Wilson Aires Ortiz[c] and César Zucco[d]

[a] *Laboratório de Bioinorgânica e Cristalografia, Departamento de Química, Universidade Federal de Santa Catarina, 88040-900, Florianópolis, SC, Brazil. E-mail: ademir@qmc.ufsc.br*
[b] *Laboratório de Efeito Mössbauer, Departamento de Física, Universidade Federal de Santa Catarina, 88040-900, Florianópolis, SC, Brazil*
[c] *Grupo de Supercondutividade e Magnetismo, Universidade Federal de São Carlos, 13565-900, São Carlos, SP, Brazil*
[d] *Laboratório de Catálise e Mecanismos de Reações Orgânicas, Departamento de Química, Universidade Federal de Santa Catarina, 88040-900, Florianópolis, SC, Brazil*

Received 25th January 2001, Accepted 26th June 2001
First published as an Advance Article on the web 17th August 2001

A new tridentate ligand [(2-hydroxybenzyl)(2-(imidazol-2-yl)ethyl)]amine (HBHA) and its first dinuclear Fe^{III} complex have been synthesized. The crystal structures of HBHA and of the complex $[Fe_2^{III}(BHA)_2(\mu\text{-}OCH_3)_2(\mu\text{-}OAc)](ClO_4)$ (**1**) have been solved by X-ray crystallography. In the cation of complex **1**, each BHA^- anion is arranged in a facial mode while one acetate and two methoxo groups as bridging ligands complete the coordination spheres of the Fe^{III} centres. The Fe^{III} ions are weakly antiferromagnetically coupled ($J = -10.1$ cm^{-1}) and undergo a quasi-reversible one-electron redox process attributed to the $Fe_2^{III}/Fe^{II}Fe^{III}$ couple. Complex **1** also displays an intense phenolate-to-Fe^{III} charge transfer transition at 517 nm ($\varepsilon = 5560$ dm^3 mol^{-1} cm^{-1}/Fe_2^{III}). The Mössbauer spectrum of **1** at 115 K shows only one quadrupole doublet, with $\delta = 0.47$ and $\Delta E_Q = 0.80$ mm s^{-1}. A comparison of the structural, magnetic and spectroscopic properties of **1** and those detected in the Fe_2^{III} form of purple acid phosphatases suggests that this compound is a potential structural model for the active site of these metalloenzymes. In addition, complex **1** also mimics some structural features found in methane monooxygenase.

Introduction

In the last few years, there has been a rapidly growing number of works employing imidazole rings in ligand design strategies. The use of phenol and imidazole rings attempts to mimic histidine and tyrosine residues, which are biologically relevant ligands that play a crucial role in several metalloenzymes, such as the purple acid phosphatases (PAPs). These enzymes comprise a family of dinuclear metal-hydrolases that have been isolated from a variety of sources including yeast, porcine uteroferrin fluid, bovine spleen, macrophages, human lysosomes and rat bones, as well as some plants and bacteria. These metalloproteins contain a dinuclear Fe^{III}–M^{II} centre (M = Fe, Mn or Zn) in their active sites, which catalyse the hydrolysis of a variety of phosphoric acid esters and anhydrides in acid conditions (pH range 4–7).[1] This group of phosphomonoesterases is also characterized by their insensitivity to tartrate inhibition and by their intense purple colour, due to the presence of a tyrosine residue ligand coordinated to a ferric ion.[2] The mammalian PAPs, the most thoroughly studied members of the class, present an antiferromagnetically spin-coupled dinuclear iron centre with two stable interconvertible states. The purple state ($\lambda_{max} = 560$ nm/$\varepsilon = 4000$ mol^{-1} dm^3 cm^{-1}) is oxidized $Fe^{III}Fe^{III}$, EPR-silent and catalytically inactive, while the pink state ($\lambda_{max} = 510$ nm/$\varepsilon = 4000$ mol^{-1} dm^3 cm^{-1}) is reduced $Fe^{III}Fe^{II}$, EPR ($g_{av} = 1.74$) and enzymatically active.[1,3]

During the last two decades, extensive studies have been carried out in attempts to uncover the active site and the functional mechanisms of these enzymes. The natural proteins have been characterized by several methods: electrochemistry,[4] resonance Raman,[5] EPR,[5,6] magnetic susceptibility,[5,7] Mössbauer,[5,8] ^{1}H NMR,[9] EXAFS[10] and kinetic studies.[11] Based on these studies and on model complexes,[12] much has been inferred with respect to the coordination active site and its implication on their catalytic activity. Recently, the structural enigma has been elucidated with the X-ray characterization of the kidney bean (kbPAP),[13,14] the rat (TRAP),[15] the rat bone[16] and uteroferrin[17] PAPs, whose similarities suggest a common mechanistic behaviour for phosphate hydrolysis.[13] The main difference between the mammalian PAP and kbPAP is that the plant enzyme is a homodimeric $Fe^{III}Zn^{II}$ metalloprotein with subunits of ≈55 kDa, whereas the mammalian enzyme is an active monomeric $Fe^{III}Fe^{II}$ (35 kDa) enzyme.

In the kbPAP enzyme (resolution 2.65 Å), the Fe^{III} ligand sphere is almost perfectly octahedral and it is comprised by the side-chains Tyr167, His325, a monodentate carboxylato group Asp135, a bridging monodentate carboxylato group Asp164 and two exogenous ligands that are modelled: a terminal hydroxo ligand (Fe–O: 1.9 Å) and a μ-hydroxo bridge (Fe–O: 1.9 Å and Zn–O: 2.1 Å). On the other hand, the zinc coordination sphere matches a distorted octahedron that, besides the bridging groups mentioned above, is coordinated

† Abbreviations used: PAPs: purple acid phosphatases; kbPAP: kidney bean purple acid phosphatase; TRAP: tartrate-resistant acid phosphatase; MMOH: methane monooxygenase; $TBAPF_6$: tetrabutylammonium hexafluorophosphate; HBHA: [(2-hydroxybenzyl)-(2-(imidazol-2-yl)ethyl)]amine; HL^3: bis(benzimidazol-2-ylmethyl)(2-hydroxyethyl)amine; TEMIMA: tris[(1-ethyl-4-methylimidazol-2-yl)-methyl]amine; TMIMA: tris[(1-methylimidazol-2-yl)methyl]amine; L^1: 1,2-bis(2,2′-bipyridyl-6-yl)ethane.

 DOI: 10.1039/b100913n

to His286, His323, one amide oxygen from Asn201 and a terminal modelled aqua ligand (Zn–O: 2.1 Å).[14] Evidencing the similarity with kbPAP, the structure of the oxidized rat bone mammalian enzyme (resolution 2.2 Å) reveals that one of the two Fe^{III} ions is ligated to the side-chains Asp35, Tyr76, His244 and an exogenous inferred solvent molecule, while the other one is coordinated to Asn112, His207, His242 and one oxygen atom from a crystallization sulfate ion. The Fe^{III} centres are also bridged by one of the carboxylato oxygen atoms, Asp73 and an oxygen atom, which, by electron density maps, may be identified as a μ-hydroxo or a μ-oxo group.[16] The coordination spheres of both Fe^{III} centres in uteroferrin (resolution 1.55 Å)[17] are close to octahedral and similar to those determined for the oxidized rat bone enzyme but with one phosphate group bridging the two metals symmetrically. Considering the presence of the histidine and tyrosine residues in the structurally characterized PAPs, we synthesized a tridentate amine ligand, [(2-hydroxybenzyl)(2-(imidazol-2-yl)ethyl)]amine (HBHA, **I**), containing imidazole and phenol moieties.

Here, we describe the syntheses, structure and characterization of the ligand, and its first Fe_2^{III} complex, $[Fe_2^{III}(BHA)_2(\mu\text{-}OCH_3)_2(\mu\text{-}OAc)](ClO_4)$ (**1**), that comprises one acetate and two methoxo exogenous bridges, as a structural model for the oxidized form of diiron PAPs. It is also worthy of note that the bis(μ-OCH_3)(μ-OAc) diiron core in complex **1** is similar to the bis(μ-OH)(μ-carboxylato) diiron core of oxidized methane monooxygenase (MMOH).[18,19]

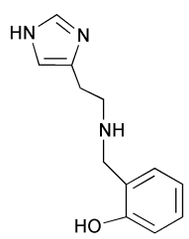

HBHA

Experimental

Materials

Histamine dihydrochloride, salicylaldehyde, iron(III) perchlorate, sodium borohydrate, and $TBAPF_6$ were purchased from Aldrich Chemical Co. Sodium acetate trihydrate and high purity solvents used in the complex synthesis and characterization were obtained from Merck and dried with molecular sieves. All other chemicals and solvents were reagent grade.

Syntheses

HBHA. The ligand was synthesized by a condensation reaction between histamine·2HCl (5.0 g, 27 mmol), previously neutralized with KOH (3.0 g, 54 mmol), and salicylaldehyde (2.8 mL, 27 mmol) in 150 mL of methanol. The reaction mixture was stirred for two hours at room temperature and then reduced by slow addition of $NaBH_4$ (1.0 g, 27 mmol) at 0 °C. The reaction mixture was concentrated under reduced pressure and the product was extracted with six 20 mL portions of $CHCl_3$. The organic extracts were combined, washed with brine, dried over $MgSO_4$, filtered and concentrated under reduced pressure resulting in a clear oil. The crude oil precipitated as a white powder by addition of propan-2-ol (5.3 g, 90%). Diffraction quality crystals of HBHA were obtained by slow recrystallization from a propan-2-ol solution. mp 122 °C. IR bands/cm^{-1}: $\nu(NH_{hist})$ 3312w; $\nu(NH_{sec})$ 3122w; $\nu(C{=}N_{hist})$ 1598s; ν(C=C) 1576s–1456s; $\delta(OH_{ph})$ 1394s; $\nu(CO_{ph})$ 1274s, $\delta(CH_{ar})$ 750s. δ_H (200 MHz; solvent $CDCl_3$; reference $SiMe_4$): 2.87 (2H, t, J = 5.9 Hz, $1CH_2$); 3.02 (2H, t, J = 5.9 Hz, $1CH_2$); 4.03 (2H, s, $1CH_2$); 4.71 (1H, br s, NH); 6.78 (1H, d, J = 7.2 Hz, CH_{ar}); 6.82 (1H, t, J = 7.7 Hz, CH_{ar}); 6.86 (1H, s, $CH_{imidazole}$); 7.00 (1H, d, J = 7.2 Hz, CH_{ar}); 7.18 (1H, t, J = 7.7 Hz, CH_{ar}); 7.60 (1H, s, $CH_{imidazole}$).

$[Fe_2^{III}(BHA)_2(\mu\text{-}OCH_3)_2(\mu\text{-}OAc)](ClO_4)$, 1. The complex was obtained by addition of $Fe(ClO_4)_3{\cdot}nH_2O$ (0.35 g, 1 mmol) to a methanolic solution of HBHA (0.22 g, 1 mmol/30 mL) and subsequent addition of $NaOAc{\cdot}3H_2O$ (0.41 g, 3 mmol). Deep red crystals suitable for X-ray structural analysis were obtained by slow evaporation of the solvent (0.23 g, 30%) (Found: C, 43.76; H, 4.99; N, 11.01. $Fe_2C_{28}H_{37}N_6O_{10}Cl$ requires: C, 43.97; H, 4.88; N, 10.99%). IR bands/cm^{-1}: $\nu(NH_{hist})$ 3252w; $\nu(C{=}N_{hist})$ 1596w; ν_{asym}(OAc) 1544s; ν_{sym}(OAc) 1452s; ν(CO) 1274vs; $\nu(ClO_4^-)$ 1112vs, 1034vs; ν_{asym}(FeOFe) 756w; ν_{sym}(FeOFe) 534w.

WARNING! Although no problems were encountered in the preparation and purification of **1**, suitable precautions should always be followed in handling perchlorate salts.

Physical measurements

Infrared spectra were recorded on a Perkin-Elmer model 16PC spectrometer, on KBr pellets in the range 4000–400 cm^{-1}. A ^1H NMR spectrum was obtained on a Bruker Ac–200F spectrometer in $CDCl_3$. Elemental analyses were performed on a Perkin-Elmer model 2400 instrument. Electronic absorption spectra were recorded on a Perkin-Elmer Lambda-19 spectrometer, in methanolic solution and in the solid state (KBr pellets). Cyclic voltammetry (CV) measurements were performed with a Princeton Applied Research (PAR) 273 system, in methanolic solution at room temperature, with 0.1 mol dm^{-3} $TBAPF_6$ as supporting electrolyte, under an argon atmosphere. These experiments were carried out employing a standard three-component system: a carbon glass working electrode, a platinum wire auxiliary electrode and an Ag/AgCl pseudo-reference electrode constructed in our laboratory. The ferrocenium–ferrocene couple was used to monitor the reference electrode.[20] Magnetic susceptibility data were obtained from the measured magnetic moment of a powder sample of the complex, over the temperature range of 2 K to 300 K, under an applied magnetic field of 0.1 Tesla. Measurements of the magnetic moment were carried out in a Quantum Design MPMS-5 SQUID magnetometer, each point being the result of two runs of 24 steps each. By use of the Pascal tables,[21] we attributed a -395.2×10^{-6} cm^3 mol^{-1} diamagnetic correction. Mössbauer spectra were measured at 298 K and 115 K against a ^{57}Co (Rh) source moving in a mode of constant acceleration. The resonance lines of the metallic iron were used for the source velocity calibration, and isomer shifts were given relative to iron metal at measured temperature.

X-Ray structural characterization

The crystal data were measured on an Enraf-Nonius CAD4 diffractometer. Unit-cell parameters were determined from centring of 25 reflections and refined by the least-squares method. Intensities were collected with graphite monochromated Mo-Kα radiation (λ = 0.71069 Å), using the ω–2θ scan technique. Three standard reflections were monitored every two hours throughout data collection and no significant intensity decay was observed. Data reductions were carried out using the HELENA computer program.[22] All diffracted intensities were corrected for Lorentz-polarization effects. The ψ scan method was employed for semi-empirical absorption correction, for complex **1** only, using the PLATON program.[23]

The structures of HBHA and complex **1** were solved by direct methods and were refined by the full-matrix least-squares method using SHELXS97[24] and SHELXL97[25] computer programs, respectively. The ZORTEP[26] program was used to generate the pictures of the molecular structures. Further

Table 1 Crystal data and structure refinement for HBHA and **1**

	1	HBHA
Formula	$C_{28}H_{37}ClFe_2N_6O_{10}$	$C_{12}H_{15}N_3O$
M	764.79	217.27
T/K	293(2)	293(2)
Crystal size/mm	0.40 × 0.23 × 0.20	0.5 × 0.3 × 0.3
Lattice type	Monoclinic	Orthorhombic
Space group	$I2/a$ (no. 15)	$P2_12_12_1$ (no. 19)
a/Å	12.540(2)	9.956(2)
b/Å	12.624(2)	10.419(2)
c/Å	41.336(8)	11.095(2)
β/°	90.69(3)	—
V/Å^3	6543.2(19)	1151.0(4)
Z	8	4
D_c/g cm^{-3}	1.553	1.254
F(000)	3168	464
θ range/°	2.48–25.00	2.68–28.48
No. of reflections collected	6464	1677
No. of unique reflections	5751	1676
No. of observed reflections [$I > 2\sigma(I)$]	3205	1118
μ/mm^{-1}	1.033	0.083
Absorption correction	ψ-scans	None
Max., min. transmission	0.97881, 0.91565	—
Parameters	452	158
Restraints	102	0
Final $R1$,[a] $wR2$[b] [$I > 2\sigma(I)$]	0.0494, 0.1219	0.0376, 0.0853
(all data)	0.1386, 0.1392	0.0852, 0.0996
Goodness-of-fit (F^2)	0.930	1.010
Extinction coefficient	—	0.020(3)
Weighting factors, a, b[c]	0.0786, 0.0000	0.0423, 0.0958
Largest diff. peak and hole/e Å^{-3}	0.922, −0.421	0.124, −0.146

[a] $R1 = \Sigma||F_o| - |F_c||/\Sigma|F_o|$. [b] $wR2 = \{\Sigma[w(F_o^2 - F_c^2)^2]/\Sigma[w(F_o^2)^2]\}^{1/2}$. [c] $w = [\sigma^2(F_o^2) + (aP)^2 + bP]^{-1}$, where $P = (F_o^2 + 2F_c^2)/3$.

crystallographic data for HBHA and complex **1** are summarized in Table 1.

HBHA. For structure determination of HBHA, 1676 unique reflections in the range $2.68 < \theta < 28.48°$ were measured, of which 1118 were considered as observed reflections. From the analysis of statistics of intensity distribution, systematic absences and successful solution and refinement of the structure, the space group of the HBHA ligand was determined to be $P2_12_12_1$ (no. 19). Hydrogen attached to C atoms, clearly revealed in a difference synthesis, were then added at their calculated positions and included in the structure factor calculations using a riding model. Other H atoms were located in the Fourier-difference map and were refined freely with isotropic thermal parameters. All non-hydrogen atoms were refined anisotropically. The following final indices were obtained after the last refinement cycle: R (on F) = 0.0376, wR (on $|F|^2$) = 0.0996 and goodness-of-fit = 1.010.

Complex 1. The structure was solved and refined in the space group $I2/a$ (no. 15). The non-standard space group was chosen to give a more orthogonal unit cell and thereby reduce correlation. The transformation matrix (1 0 1/0 1 0/−1 0 0) yielded the standard space group $C2/c$ with cell constants $a = 43.052$ Å, $b = 12.624$ Å, $c = 12.540$ Å and $\beta = 106.243°$. 6464 reflections were collected in the range $2.48 < \theta < 25.00°$, 5751 of which were non-equivalent by symmetry [R_{int} (on I) = 0.0387] (very negative intensities were ignored). All non-hydrogen atoms were refined with anisotropic displacement parameters. H atoms were computed and refined with an isotropic thermal parameter using a riding model, except for H7, bonded to N7, which was found from Fourier-difference synthesis and refined as a free atom. The perchlorate anion exhibits a rotational disorder about its molecular threefold axis, where each of the three oxygen atoms are disordered over two positions with 0.6 and 0.4 occupancies. The final R (on F) factor was 0.0494, wR (on $|F|^2$) = 0.1391 and goodness-of-fit = 0.930.

CCDC reference numbers 157480 and 157481.

See http://www.rsc.org/suppdata/dt/b1/b100913n/ for crystallographic data in CIF or other electronic format.

Results and discussion

Syntheses

The N,O-donor ligand HBHA was readily obtained in good purity and yield by the procedure described herein, and its characterization was unambiguously established by X-ray analysis and IR and ^{1}H NMR spectroscopies.

The ligand reacts in methanol with $Fe(ClO_4)_3 \cdot nH_2O$ and $NaOAc \cdot 3H_2O$, in a 1 : 1 : 3 stoichiometry, producing complex **1**. The IR spectrum of **1** is similar to that of the free ligand HBHA and it differs only in: a) the appearance of two bands at 1544 and 1452 cm^{-1}, with $\Delta \approx 92$ cm^{-1}, attributed to the ν_{asym} and ν_{sym} stretching modes of the acetate anion coordinated to the Fe^{III} centres in the bridging form,[27] b) the bands at 1112 and 1034 cm^{-1} attributed to the perchlorate counter-ion,[27] c) the bands at 756 and 534 cm^{-1} that could be attributed to the ν_{asym} and ν_{sym} Fe–O–Fe stretching,[28] respectively, and d) the absence of the band at 1354 cm^{-1} attributed to the δ(O–H) mode, indicating that the phenol groups are coordinated in the deprotonated form.

Molecular structures

The colourless monocrystals of HBHA belong to the orthorhombic system, space group $P2_12_12_1$. ZORTEP[26] views of the molecular structure and the intermolecular hydrogen bonding of the ligand HBHA are shown in Fig. 1. Fig. 1(a) shows the free tridentate amine ligand HBHA, with phenol and histamine pendant arms. The N–C distances N(8)–C(9): 1.470(3) Å and N(8)–C(7): 1.476(3) Å are consistent with amine–carbon (sp^3) bond lengths and are similar to those detected in complex **1**: N(21)–C(30): 1.496(6) Å and N(21)–C(22): 1.477(6) Å. The structure of HBHA reveals that a significant rearrangement

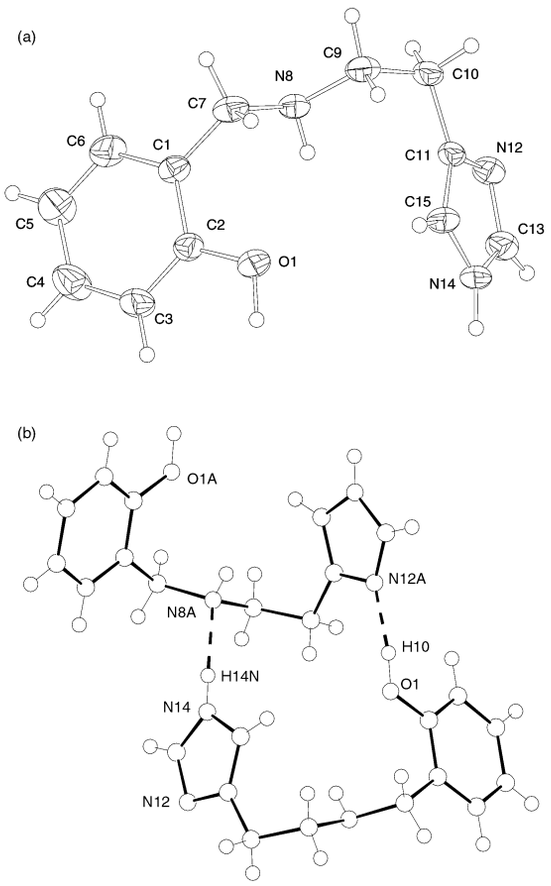

Fig. 1 (a) A view of the molecular structure of HBHA showing the atom numbering scheme. Ellipsoids are drawn at the 40% probability level. Selected bond lengths (Å) and angles (°): N(8)–C(9) 1.470(3); N(8)–C(7) 1.476(3); N(14)–C(13) 1.331(3); N(14)–C(15) 1.359(3); C(11)–N(12) 1.363(3); N(12)–C(13) 1.326(3); C(9)–N(8)–C(7) 113.34(19); C(13)–N(14)–C(15) 107.31(18); C(13)–N(12)–C(11) 105.61(19). (b) Hydrogen bond interactions: N(14)–H(14N) 0.90(2) Å; H(14)···N(8)^{i} 1.96(2) Å; N(14)···N(8)^{i} 2.855(3) Å; N(14)–H(14N)···N(8)^{i} 173(3)°; O(1)–H(10) 0.98(3) Å; H(10)···N(12)^{i} 1.76(3) Å; O(1)···N(12)^{i} 2.726(3) Å; O(1)–H(10)···N(12)^{i} 170(3)°. Symmetry code: i: $1 - x$, $1/2 + y$, $3/2 + z$.

must occur in the ligand to achieve the normal coordination mode of a tridentate ligand in a facial arrangement. This conformational rearrangement can be observed in the large O(1)···N(12) donor-atom distance of 5.643(3) Å, which should be compared with the value of 2.972(5) Å, in the Fe(2) centre and 3.026(5) Å, in the Fe(1) centre, when the ligand is coordinated to the Fe^{III} centres in complex **1**.

Fig. 1(b) shows that there are two intermolecular hydrogen interactions: N(14)···N(8)^{i}: 2.855(3) Å, N(14)–H(14N)···N(8)^{i}: 173(3)° and O(10)···N(12)^{i}: 2.726(3) Å, O(1)–H(10)···N(12)^{i}: 170(3)°, symmetry code: i: $1 - x$, $1/2 + y$, $3/2 + z$, that maintain the relatively compact conformation adopted by the molecule in the solid state. These hydrogen contacts are responsible for the conformational arrangement adopted by the histamine ring in the free ligand when compared with that observed in complex **1**, as discussed above. The red crystals of formula $[Fe_2^{III}(BHA)_2(\mu\text{-}OCH_3)_2(\mu\text{-}OAc)](ClO_4)$ **1**, belong to the monoclinic system, space group *I*2/*a*. A ZORTEP[26] view of the cation complex is shown in Fig. 2. The cation complex consists of a diiron dimer, with both hexacoordinated Fe^{III} ions in distorted octahedral environments. All angles around the metal centres that deviate from 180° and 90°, as observed in the legend of Fig. 2, evidence this distortion. The ligand is arranged in a facial mode, forming two six-membered rings with the phenol and the histamine arms, that

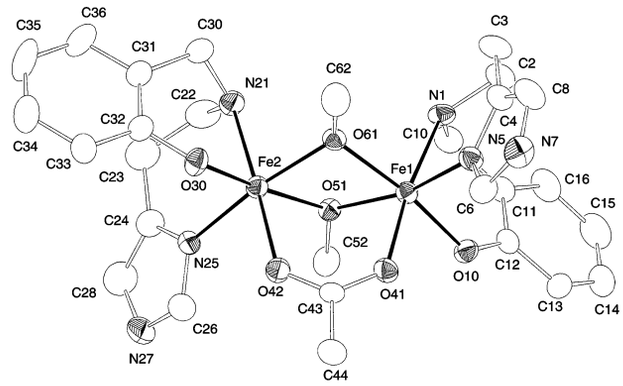

Fig. 2 Molecular structure of $[Fe_2^{III}(BHA)_2(\mu\text{-}OCH_3)_2(\mu\text{-}OAc)]^+$ with the atom numbering scheme. Ellipsoids are drawn at the 40% probability level. Hydrogen atoms have been omitted for clarity. Selected bond lengths (Å) and angles (°): Fe(2)–O(30) 1.925(3); Fe(2)–O(61) 1.986(3); Fe(2)–O(51) 2.037(3); Fe(2)–O(42) 2.058(3); Fe(2)–N(25) 2.115(4); Fe(2)–N(21) 2.151(4); Fe(2)···Fe(1) 3.1047(11); Fe(1)–O(10) 1.922(3); Fe(1)–O(51) 1.996(3); Fe(1)–O(61) 2.029(3); Fe(1)–O(41) 2.061(3); Fe(1)–N(5) 2.104(4); Fe(1)–N(1) 2.155(4); O(10)–Fe(1)–O(51) 97.89(13); O(10)–Fe(1)–O(61) 171.74(13); O(51)–Fe(1)–O(61) 74.61(12); O(10)–Fe(1)–O(41) 86.42(13); O(51)–Fe(1)–O(41) 92.61(12); O(61)–Fe(1)–O(41) 90.42(12); O(10)–Fe(1)–N(5) 97.37(14); O(51)–Fe(1)–N(5) 164.72(13); O(61)–Fe(1)–N(5) 90.12(14); O(41)–Fe(1)–N(5) 87.57(13); O(10)–Fe(1)–N(1) 88.46(14); O(51)–Fe(1)–N(1) 93.29(13); O(61)–Fe(1)–N(1) 95.34(13); O(41)–Fe(1)–N(1) 172.67(13); N(5)–Fe(1)–N(1) 87.88(15); O(30)–Fe(2)–O(61) 98.80(13); O(30)–Fe(2)–O(51) 173.18(13); O(61)–Fe(2)–O(51) 74.63(11); O(30)–Fe(2)–O(42) 88.83(13); O(61)–Fe(2)–O(42) 93.07(12); O(51)–Fe(2)–O(42) 89.70(12); O(30)–Fe(2)–N(25) 94.61(14); O(61)–Fe(2)–N(25) 166.53(14); O(51)–Fe(2)–N(25) 92.01(13); O(42)–Fe(2)–N(25) 88.49(14); O(30)–Fe(2)–N(21) 91.68(14); O(61)–Fe(2)–N(21) 89.74(14); O(51)–Fe(2)–N(21) 90.13(13); O(42)–Fe(2)–N(21) 177.03(14); N(25)–Fe(2)–N(21) 88.55(15); Fe(1)–O(51)–Fe(2) 100.68(13); Fe(2)–O(61)–Fe(1) 101.27(13).

for Fe(2) centre shows the following bite angles: O(30)–Fe(2)–N(21): 91.68(1)° and N(25)–Fe(2)–N(21): 88.55(1)°. The arrangement of the ligand BHA^- around the Fe(1) centre is similar and slight deviations from 90° are a result of the ligand chelate effect. The oxygen atoms from the acetate and the two methoxo groups triply bridge the two Fe^{III} centres. Thus, the coordination sphere around each Fe^{III} atom is the same and an N_2O_4 donor set of atoms comprises each one.

In the Fe(2) centre, the N(25) imidazole nitrogen atom is *trans* to the O(61) methoxo bridge oxygen atom, and *cis* with respect to the other two oxygen atoms: one from a phenolate group O(30) and the other from another methoxo bridge O(51). Completing the octahedral coordination spheres around Fe(1) and Fe(2) centres, the amine nitrogen atoms N(1) and N(21) are *trans* to the O(41) and O(42) acetate oxygen atoms, respectively. The Fe···Fe distance [3.105(1) Å] in **1** is similar to those reported for some complexes where the alkoxo bridges are derived from the methanol, ethanol and *n*-propanol alcohols,[29–32] as shown in Table 2. This Fe···Fe distance also compares favourably to the values reported for the purple acid phosphatase from mammalian rat TRAP (3.1 Å)[15] and the oxidized form of methane monooxygenase [2.99–3.07 Å][18,19] containing the bis(μ-OH)(μ-carboxylato) diiron core. Importantly, a dinuclear Fe^{III} complex having the unprecedented *trans*,*trans*-bis(μ-OH)bis(μ-carboxylato) diiron core has been reported recently as a structural and functional model for MMOH, but with significantly shorter Fe···Fe distance (av. 2.86 Å) than that detected in the triply bridged complex **1**.[33] The Fe–O–Fe methoxo bridging angles are also close to the values reported for the analogous complex $[Fe_2(\mu\text{-}OMe)_2Cl_2(O_2CPh)L^1]$[29] and to other di(μ-methoxo) and di(μ-ethoxo) complexes[30–32] (Table 2). Nevertheless, these angles are smaller than those observed in some complexes that contain phenoxo

Table 2 Structural and magnetic data for some Fe_2^{III} complexes

Complex	Fe···Fe/Å	Fe–O–Fe[a]/°	Fe–O_{bridge}[a]/Å	Fe–O_{ph}/Å	J_{exp}/cm^{-1}	Ref.
$[Fe_2(\mu\text{-}OCH_3)_2(BHA)_2(OAc)]^{+}$ [b]	3.105	101	2.013 2.012	1.922 1.925	−10.1	This work
$[Fe_2(\mu\text{-}OCH_3)_2Cl_2(O_2CPh)L^1]$ [c]	3.088	101.8	1.987 1.993	—	−10.5	29
$[Fe_2L^2(\mu\text{-}OCH_3)_2]$ [d]	3.162	103.7	2.01	1.919 1.930	—	30
$[Fe(\mu\text{-}OCH_3)(DBM)_2]_2$ [e]	3.087	102.0	1.987	—	+15.4	31
$[Fe(\mu\text{-}OCH_3)(DPM)_2]_2$ [f]	3.105	103.7	1.977	—	+19.0	31
$[Fe(\mu\text{-}OEt)(BPM)_2]_2$ [g]	3.049	101.8	1.965	—	+14.8	31
$[Fe(\mu\text{-}OPr)(NPM)_2]_2$ [h]	3.093	103.1	1.974	—	+18.0	31
$[Fe_2L^4(\mu\text{-}OCH_3)Cl_2]$ [i]	3.097	101	1.98 1.995	—	−16.3	32*a*
$[Fe_2L(\mu\text{-}OEt)_2Cl_2]$ [j]	3.144	104.3	1.991	—	−15.4	32*b*
$[Fe_2(ACAC)_4(\mu\text{-}OEt)_2]$	3.116	103.6	1.982	—	−11.0	32*b*
$[Fe_2(L^5)_2(\mu\text{-}OCH_3)_2]$ [k]	3.168	104.5	2.002	—	−10.9	32*c*
$[PH(t\text{-}Bu)_3]_2[Fe_2(\mu\text{-}OEt)_2Cl_6]$	3.177	107.0	1.976	—	−24.6	32*d*
$[Fe_2(L^A)(\mu\text{-}OCH_3)(Cl_2)_2(CH_3OH)]$ [l]	3.140	102.9	2.008	1.983	−10.6	32*e*
$[\{Fe(3,6\text{-}DBSQ)_2(\mu\text{-}OCH_3)\}_2]$ [m]	3.093	103.2	1.974	—	−22.4	32*f*
$Fe_2(\mu\text{-}OCH_3)_2(CHP)_4(DMBIPY)_2$ [n]	3.194	104.7	2.016 2.045	—	−26.8	32*g*
$[Fe_2(\mu\text{-}OCH_3)_2(CHP)_4(PHEN)_2]$	3.153	104.3	1.997 2.045	—	−28.6	32*g*
$[Fe_2(BIOMP)(O_2CCH_3)_2]ClO_4$ [o]	3.567	117.5	2.089	1.876	−6.4	34
$[Fe_2(BBPMP)(O_2CCH_3)_2]ClO_4$ [p]	3.528	118.3	2.055	1.861	−6.0	35
$[Fe_2(TPDB)(C_6H_5CO_2)]ClO_4$ [q]	3.300	111.2	2.01	—	−10.7	36
$[Fe_2(BPClNOL)_2(OAc)]ClO_4$ [r]	3.041	98.3	2.015 2.002	1.859 1.885	−3.9	37
$[Fe_2(BPClNOL)_2(H_2O)_2]ClO_4$	3.122	101.95	2.089	—	−4.8	37
$[Fe_2(BHPP)(O_2P(OPh)_2)_2]BF_4$ [s]	3.549	124.0	2.01	1.855	−12.5	38
$[Fe_2(BHPMP)(O_2P(OPh)_2)_2]ClO_4$ [t]	3.837	128.2	2.133	1.852 1.854	−5.6	38
$[Fe_2(BBPMP)(SO_4)_2]$	3.624	121.7	2.075	1.94	−6.4	39

[a] Average value. [b] HBHA: [(2-hydroxybenzyl)(2-(imidazol-2-yl)ethyl)]amine. [c] L^1: 1,2-bis(2,2′-bipyrid-6-yl)ethane. [d] H_2L^2: 1,2-Bis(2′-hydroxybenzyl)ethane-1,2-diamine. [e] HDBM: Dibenzoylmethane. [f] HDPM: Dipivaloylmethane. [g] HBPM: Benzoylpivaloylmethane. [h] HNMP: Naphthoylpivaloylmethane. [i] H_2L^4: 1,4-Piperazinebis(*N*-ethylenesalicylaldimine). [j] HL: 1,4-Piperazinediyl-bis(*N*-ethylenesalicylaldimine). [k] H_2L^5: Pimelyl-bis(*N*-isopropylhydroxamic acid). [l] H_3L^A: *N*,*N*′-Bis(salicylidene-1,3-propan-2-ol). [m] 3,6-DBSQ: 3,6-Di-*tert*-butyl-1,2-benzoquinone. [n] HCHP: 6-Chloro-2-pyridone, DMBIPY: 4,4′-Dimethyl-2,2′-bipyridine. [o] H_3BIOMP: 2,6-Bis[((2-hydroxybenzyl)((1-methylimidazol-2-yl)methyl)amino)methyl]-4-methylphenol. [p] H_3BBPMP: 2,6-Bis[((2-hydroxybenzyl)(2-pyridylmethyl)amino)methyl]-4-methylphenol. [q] TPDB: *N*,*N*,*N*′,*N*′-Tetrakis(2-pyridylmethyl)-1,4-diaminobutane-2-olate. [r] H_2BPClNOL: *N*-(2-Hydroxybenzyl)-*N*-(2-pyridylmethyl)[(3-chloro)-(2-hydroxy)]propylamine. [s] H_3BHPP: 1,3-Bis[(2-hydroxybenzyl)(2-pyridylmethyl)amino]-2-propanol. [t] H_3BHPMP: 2,6-Bis[(2-hydroxybenzyl)-(2-pyridylmethyl)amino)methyl]-4-methylphenol.

or alkoxo bridges as endogeneous ligands [34–39] (Table 2) and this is a consequence of the five- and six-membered chelate rings formed with the 2,6-bis(aminomethyl)-4-methylphenol and 1,3-diamine-2-propanol moieties. The Fe–O bond lengths of the methoxo bridges are very close to those reported for the complex $[Fe_2(\mu\text{-}OMe)_2Cl_2(O_2CPh)L^1]$ [29] and are in the mid-range observed for other related di(μ-methoxo) and di(μ-ethoxo) diiron complexes [30–32] given in Table 2. The amine Fe–N lengths [Fe(1)–N(1): 2.155(4) Å and Fe(2)–N(21): 2.151(4) Å] are the longest of the coordination sphere. The Fe–N lengths from the histamine rings [Fe(2)–N(25): 2.115(4) Å and Fe(1)–N(5): 2.104(4) Å] are similar to the values reported for some Fe^{III}–N complexes with correlated imidazole rings, such as: $[\{FeL_3[O_2P(OPh)_2]\}_2](ClO_4)_2$: Fe(1)–N(2): 2.10(1) Å;[28] $[Fe_2(BIOMP)(O_2CCH_3)_2](ClO_4)$: Fe(1)–N(2): 2.094(9) Å;[34] $Fe_2O(TEMIMA)(TMIMA)(OAc)](ClO_4)_3$: Fe(1)–N(6): 2.15(1) Å;[40] which have benzimidazole, 1-methylimidazole and 1-ethyl-4-methylimidazole as N-donor groups, respectively. The $Fe–O_{phenolate}$ distances [Fe(1)–O(10): 1.922(3) Å and Fe(2)–O(30): 1.925(3) Å] are slightly longer than those reported for the complexes in which the phenolate groups are *trans* to alkoxo or phenoxo bridges [34–36] (Table 2). The $Fe–O_{acetate}$ lengths [Fe(1)–O(41): 2.061(3) and Fe(2)–O(42): 2.058(3) Å] are typical for acetate bridges. Finally, since in recent years the molecular structures of the purple acid phosphatases from mammalian sources,[15–17] and the kidney bean (resolution 2.65 Å) [13,14] have been solved, a comparison with these is relevant. As described above, the Fe^{III} centres in complex **1** are coordinated to the phenol oxygen and histamine nitrogen atoms, which perfectly mimic the tyrosine and the histidine residues present in these enzymes. In addition, the methoxo and the acetate bridges should mimic the inferred hydroxo and the aspartate residue bridges, respectively. It should be noted that the Fe–OMe bond lengths in **1** [av. Fe–O(61) = 2.007 Å and Fe–O(51) = 2.016 Å] are very similar to the Fe–O distances of 2.0 Å postulated as a hydroxo bridge in PAPs from rat bone (resolution 2.2 Å) [16] and uteroferrin (resolution 1.55 Å).[17] The $Fe–O_{phenolate}$ (av. 1.924 Å) bond lengths are slightly smaller but are also comparable to the $Fe–O_{Tyr}$ (1.98 Å) in uteroferrin.[17] Finally, the $Fe–N_{His}$ distance at the same Fe^{III} centre in the enzyme is ~0.2 Å longer than the corresponding $Fe–N_{imidazole}$ bond lengths in **1**.

Magnetochemistry and Mössbauer studies

The temperature dependence of the magnetic susceptibility and effective magnetic moment (μ_{eff}) is shown in Fig. 3. The μ_{eff} value per dimer is 7.12 μ_B at 298 K, indicating the presence of high spin Fe^{III} species, and falls to 0.31 μ_B at 2 K according to an antiferromagnetic intramolecular coupling. The susceptibility curve analysis was obtained using the isotropic spin–spin interaction by the Heisenberg–Dirac–Van Vleck Hamiltonian, $H = -JS_1S_2$, where $S_1 = S_2 = 5/2$. Solving the Van Vleck equation for this Hamiltonian, results in the following magnetic susceptibility equation,[21] which was used to fit the experimental data:

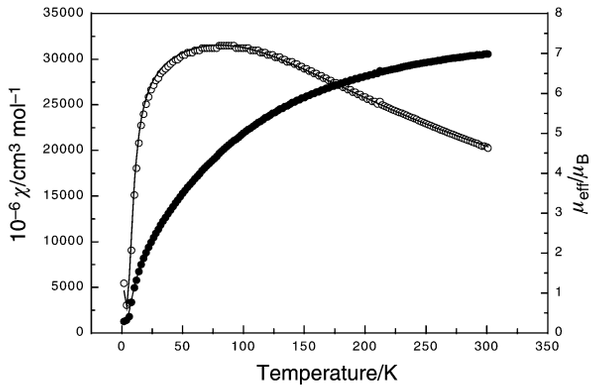

Fig. 3 Temperature dependence of the magnetic susceptibility (χ) and effective magnetic moment (μ) per iron of complex **1**.

$$\chi = (1 - x_p)\frac{N_A\mu_B^2}{k(T-\Theta)}g^2 \times \left[\frac{2e^{2x} + 10e^{6x} + 28e^{12x} + 60e^{20x} + 110e^{30x}}{1 + 3e^{2x} + 5e^{6x} + 7e^{12x} + 9e^{20x} + 11e^{30x}}\right] + 2x_p\frac{N_A\mu_B^2}{3k(T-\Theta)}g^2 S(S+1) + 2\text{TIP}$$

$$\text{with, } x = \frac{J}{kT}$$

where, N_A: Avogadro constant; μ_B: Bohr magneton; x_p: paramagnetic fraction per monomer; g: spectroscopic splitting factor; k: Boltzmann constant; Θ: Weiss temperature; TIP: temperature independent paramagnetism per monomer. The best-fit parameters found were: $J = -10.1 \pm 0.1$ cm^{-1}, $g = 2.00$ (fixed), TIP = 100×10^{-6} cm^3 mol^{-1} and paramagnetic fraction = 0.15%. The low value for the paramagnetic fraction indicates a small number of magnetically non-coupled units, reflecting the good crystallinity of the material. The $J = -10.1 \pm 0.1$ cm^{-1} value is very close to that reported for the complex $[Fe_2(\mu\text{-OMe})_2Cl_2(O_2CPh)L^1]$ **2**: $J = -10.5$ cm^{-1},[29] which contains a similar tribridged structure composed by the di(μ-methoxo)(μ-benzoate) core and to that shown by the complex $[Fe^{III}_2(BBPMP)(\mu\text{-OAc})(\mu\text{-OH})]ClO_4$: $J = -10.6$ cm^{-1},[35] in which the bridging core comprises one phenoxo, one acetate and one hydroxo groups. The J value also lies in the middle range of values reported for di(μ-methoxo) and di(μ-ethoxo) complexes[30–32] (Table 2) and is in the range $-6 \leq J \leq -15$ cm^{-1} found for the oxidized form of purple acid phosphatases.[7] As in complex **1**, the long $Fe^{III}(OH)Fe^{III}$ bond distances (2.0 Å) must probably account for the weak antiferromagnetic coupling in PAPs. The experimental antiferromagnetic interactions observed for the complexes **1** and **2** are consistent with the expected J values (**1**: -7.5 cm^{-1} and **2**: $J = -10.9$ cm^{-1}) calculated from the empirical Gorun and Lippard equation.[41] As can be observed, these values show a difference of three units between them, which could be explained by the slight difference in the Fe–O–Fe pathway distances (P) from methoxo bridges, since the Gorun and Lippard [41] model only employs the structural P parameter for the J value prediction.

The ^{57}Fe Mössbauer spectra of **1** were recorded at 298 and 115 K and are shown in Fig. 4. Both spectra display a single quadrupole-split doublet, with an isomer shift (δ) of 0.37(1) mm s^{-1} at 298 K and 0.47(1) mm s^{-1} at 115 K. The quadrupole splitting (ΔE_Q) is the same at 298 K and at 115 K and is equal to 0.80(1) mm s^{-1}. These parameters indicate a single type of high-spin Fe^{III} centre and the existence of octahedral high-spin Fe^{III} ions observed in the structure and magnetic analysis.[42]

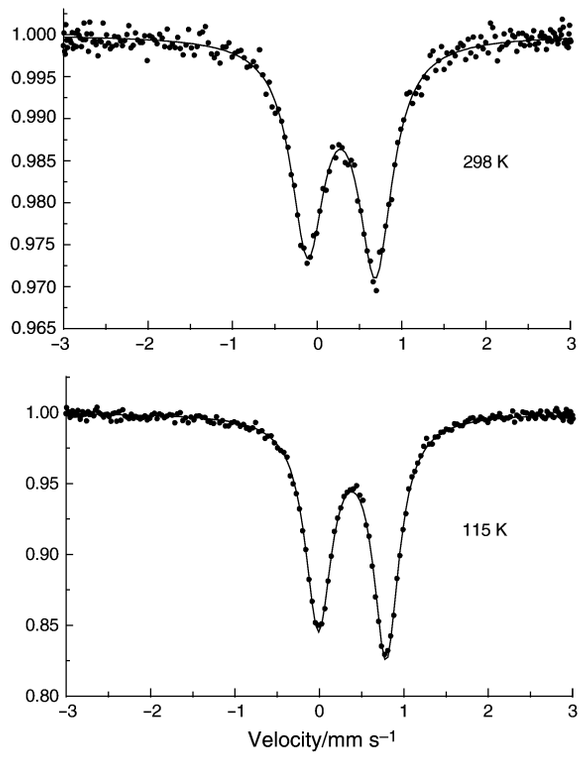

Fig. 4 ^{57}Fe Mössbauer spectra of a polycrystalline sample of complex **1** at 298 and 115 K.

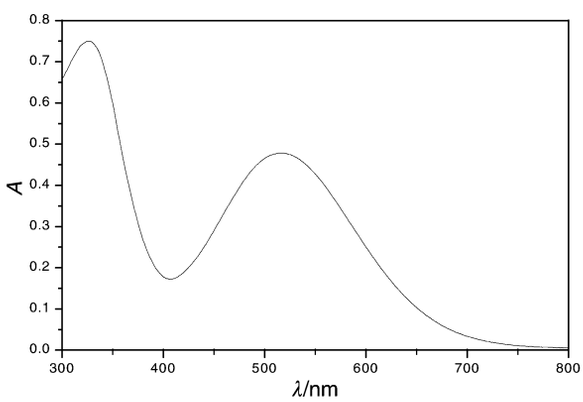

Fig. 5 UV-Visible absorption spectra of complex **1**, in CH_3OH (8.6×10^{-5} mol dm^{-3}), at room temperature.

UV-Vis spectroscopy and electrochemistry

The electronic behaviour of **1** was investigated in the solid state by the reflectance technique and in methanolic solution. In both cases, the spectra clearly show the following transitions: λ_{max}/nm (CH_3OH) 517 (ε/dm^3 mol^{-1} cm^{-1} 5560) and 327 (8730) and (KBr-pellets) 512 and 318 (Fig. 5). The two absorption bands display intense molar absorption coefficients that may be ascribed as phenolate to Fe^{III} charge transfer transitions (LMCT), since high-spin Fe^{III} ions, under an octahedral crystal field, should show only very weak d–d absorption bands due to spin forbidden transitions. The former band is assigned to a transition from the pπ orbital on the phenolate oxygen to the half-filled dπ* orbital on the ferric ion, similar to oxidized PAPs[5] and related model compounds,[34–36] while the latter is assigned to the half-filled dσ* orbital on the ferric ion.[43] The similarities between the absorption maxima values in methanolic solution and in the solid state indicate that the complex structure does not undergo solvent influence in this case and that its integrity is maintained in solution.

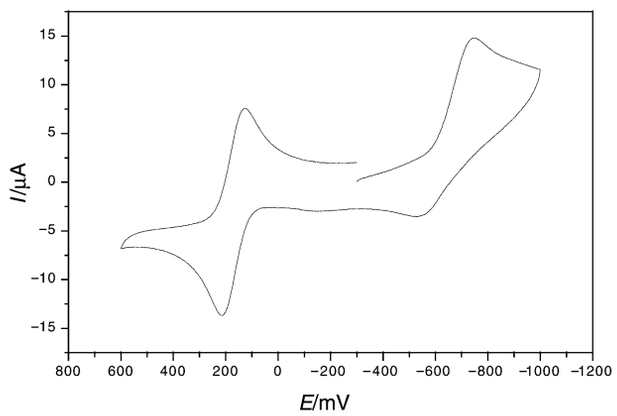

Fig. 6 Cyclic voltammogram of complex **1** in CH_3OH [0.1 mol dm^{-3} $TBAPF_6$ as supporting electrolyte, glassy carbon working electrode (diameter 3 mm), ferrocene as internal standard, scan rate of 50 mV s^{-1}].

In view of this, the redox properties of complex **1** were investigated by cyclic voltammetry in methanolic solution (Fig. 6). One quasi-reversible wave was observed at −0.41 V *vs.* NHE (−0.81 V *vs.* Fc^+/Fc), which could be attributed to an Fe_2^{III} to $Fe^{III}Fe^{II}$ redox process. Unfortunately, this value may not be compared to the di(μ-methoxo) complexes listed in Table 2, since no electrochemical data have been reported for these species. On the other hand, this $E_{1/2}$ value compares very well with the corresponding $Fe_2^{III}/Fe^{III}Fe^{II}$ redox couple in the $[Fe_2(BIOMP)(OAc)_2]^+$ complex ($E_{1/2} = -0.355$ V *vs.* NHE)[34] which contains one phenolate and one 1-methylimidazole group terminally bonded to the Fe^{III} centres. However, these $E_{1/2}$ values are cathodically shifted when compared to the reported value of +0.367 *vs.* NHE at pH 5.0 for uteroferrin,[4] which has only one terminal phenolate coordinated to the non-reducible Fe^{III} centre, while in the complexes there is one terminal phenolate ligand on each Fe^{III} centre. In summary, we have synthesized and fully characterized a dinuclear Fe^{III} complex with the new tridentate HBHA ligand, which contains phenolate and imidazole donor groups. The complex $[Fe_2^{III}(BHA)_2(\mu\text{-}OCH_3)_2(\mu\text{-}OAc)](ClO_4)$ (**1**), represents a rare example of a diiron(III) complex triply bridged by two methoxo and one acetate exogenous groups,[29] which parallels closely the $(\mu\text{-}OH)_2$-(μ-carboxylato) structural core and the $Fe^{III} \cdots Fe^{III}$ distance of the hydroxylase component of MMOH.[18,19] Moreover, the coordination environment of the Fe^{III} centres and the magnetic and spectroscopic properties indicate that **1** can be considered as a potential structural model for the oxidized form of purple acid phosphatases.

Acknowledgements

This work was supported by grants from Capes, CNPq and PRONEX.

References

1 K. Doi, B. C. Antanaitis and P. Aisen, *Struct. Bonding (Berlin)*, 1988, **70**, 1; T. Klabunde and B. Krebs, *Struct. Bonding (Berlin)*, 1997, **89**, 177.
2 B. C. Antanaitis and P. Aisen, *Adv. Inorg. Biochem.*, 1983, **5**, 111; B. C. Antanaitis, T. Strekos and P. Aisen, *J. Biol. Chem.*, 1982, **257**, 3766.
3 J. B. Vincent, M. W. Crowder and B. A. Averill, *Biochemistry*, 1991, **30**, 3025.
4 D. L. Wang, R. C. Holz, S. S. David, L. Que, Jr. and M. T. Stankovich, *Biochemistry*, 1991, **30**, 8187.
5 B. A. Averill, J. C. Davis, S. Burman, T. Zirino, J. S. Loehr, T. M. Loehr, J. T. Sage and P. G. Debrunner, *J. Am. Chem. Soc.*, 1987, **109**, 3760.
6 B. C. Antanaitis, P. Aisen and H. R. Lilienthal, *J. Biol. Chem.*, 1983, **258**, 3166; M. W. Crowder, J. B. Vincent and B. A. Averill, *Biochemistry*, 1992, **31**, 9603.
7 S. Gehring, P. Fleischhauer, M. Behlendorf, M. Hüber, J. Lorösch, W. Haase, M. Dietrich, H. Witzel, R. Löcke and B. Krebs, *Inorg. Chim. Acta*, 1996, **252**, 13.
8 P. G. Debrunner, M. P. Hendrich, J. Jersey, D. T. Keough, J. T. Sage and B. Zerner, *Biochim. Biophys. Acta*, 1983, **745**, 103; J. H. Rodriguez, H. N. Ok, Y.-M. Xia, P. G. Debrunner, B. E. Hinrichs, T. Meyer and N. H. Packard, *J. Phys. Chem.*, 1996, **100**, 6849.
9 R. C. Scarrow, J. W. Pyrz and L. Que, Jr., *J. Am. Chem. Soc.*, 1990, **112**, 657; R. B. Lauffer, B. C. Antanaitis, P. Aisen and L. Que, Jr., *J. Biol. Chem.*, 1983, **258**, 14212.
10 A. E. True, R. C. Scarrow, C. R. Randall, R. C. Holz and L. Que, Jr., *J. Am. Chem. Soc.*, 1993, **115**, 4246; S. Priggemeyer, P. E. Borkenstein, F. Ahlers, G. Henkel, M. Körner, H. Witzel, H.-F. Nolting, C. Hermes and B. Krebs, *Inorg. Chem.*, 1995, **34**, 1445.
11 M. A. S. Aquino, J.-S. Lim and G. Sykes, *J. Chem. Soc., Dalton Trans.*, 1992, 2135; E. G. Mueller, M. W. Crowder, B. A. Averill and J. R. Knowles, *J. Am. Chem. Soc.*, 1993, **115**, 2974; M. A. S. Aquino, J.-S. Lim and A. G. Sykes, *J. Chem. Soc., Dalton Trans.*, 1994, 429; M. A. S. Aquino and A. G. Sykes, *J. Chem. Soc., Dalton Trans.*, 1994, 683.
12 R. Than, A. A. Feldmann and B. Krebs, *Coord. Chem. Rev.*, 1999, **182**, 211.
13 T. Klabunde, N. Sträter, R. Fröhlich, H. Witzel and B. Krebs, *J. Mol. Biol.*, 1996, **259**, 737.
14 N. Sträter, T. Klabunde, P. Tucker, H. Witzel and B. Krebs, *Science*, 1995, **268**, 1489.
15 J. Uppenberg, F. Lindqvist, C. Svensson, B. Ek-Rylander and G. Anderson, *J. Mol. Biol.*, 1999, **290**, 201.
16 Y. Lindqvist, E. Johansson, H. Kaija, P. Vihko and G. Schneider, *J. Mol. Biol.*, 1999, **291**, 135.
17 L. W. Guddat, A. S. McAlpine, D. Hume, S. Hamilton, J. Jersey and J. L. Martin, *Structure*, 1999, **7**, 757.
18 N. Elango, R. Radhakrushnan, W. A. Froland, B. J. Wallar, C. A. Earhart, J. D. Lipscomb and D. H. Ohlendorf, *Protein Sci.*, 1997, **6**, 556.
19 A. C. Rosenzweig, H. Branstetter, D. A. Whittihgton, P. Nordlund, S. J. Lippard and C. A. Frederick, *Proteins: Struct., Funct. Genet.*, 1997, **29**, 141.
20 R. R. Gagné, C. A. Koval and G. C. Lisensky, *Inorg. Chem.*, 1980, **19**, 2854.
21 C. J. O'Connor, *Prog. Inorg. Chem.*, 1982, **29**, 203.
22 A. L. Spek, HELENA, Program for Reduction of CAD-4 Data, University of Utrecht, The Netherlands, 1996.
23 A. L. Spek, *Acta Crystallogr., Sect. A*, 1990, **46**, C34.
24 G. M. Sheldrick, SHELXS97, Program for the Solution of Crystal Structures, University of Göttingen, Germany, 1997.
25 G. M. Sheldrick, SHELXL97, Program for the Refinement of Crystal Structures, University of Göttingen, Germany, 1997.
26 L. Zsolnai, H. Pritzkow and G. Hutter, ZORTEP, University of Heidelberg, Germany, 1996.
27 K. Nakamoto, in *Infrared and Raman Spectra of Inorganic and Coordination Compounds*, 3rd edn., John Wiley & Sons, NY, 1977, part III, pp. 231, 232, 242.
28 L. Yin, P. Cheng, X. Yao and H. Wang, *J. Chem. Soc., Dalton Trans.*, 1997, 2109.
29 C. M. Grant, M. J. Knapp, W. E. Streib, J. C. Huffman, D. N. Hendrickson and G. Christou, *Inorg. Chem.*, 1998, **37**, 6065.
30 R. Viswanathan, M. Palaniandavar, P. Prabakaran and P. T. Muthiah, *Inorg. Chem.*, 1998, **37**, 3881.
31 F. Le Gall, F. F. Biani, A. Caneschi, P. Cinelli, A. Cornia, A. C. Fabretti and D. Gatteschi, *Inorg. Chim. Acta*, 1997, **262**, 123.
32 (*a*) B. Chiari, O. Piovesana, T. Tarantelli and P. F. Zanazzi, *Inorg. Chem.*, 1982, **21**, 1396; (*b*) B. Chiari, O. Piovesana, T. Tarantelli and P. F. Zanazzi, *Inorg. Chem.*, 1984, **23**, 3398; (*c*) S. J. Barclay, P. E. Riley and K. N. Raymond, *Inorg. Chem.*, 1984, **23**, 2005; (*d*) J. D. Walker and R. Poli, *Inorg. Chem.*, 1990, **29**, 756; (*e*) G. D. Fallon, A. Markiewicz, K. S. Murray and T. Quach, *J. Chem. Soc., Chem. Commun.*, 1991, 198; (*f*) A. S. Attia, B. J. Conklin, C. W. Lange and C. G. Pierpont, *Inorg. Chem.*, 1996, **35**, 1033; (*g*) A. J. Blake, C. M. Grant, S. Parsons, G. A. Solan and R. E. P. Winpenny, *J. Chem. Soc., Dalton Trans.*, 1996, 321.
33 L. Dongwhan and S. J. Lippard, *J. Am. Chem. Soc.*, 1998, **120**, 12153.
34 H. Nie, S. M. J. Aubin, M. S. Mashuta, C.-C. Wu, J. F. Richardson, D. N. Hendrickson and R. M. Buchanan, *Inorg. Chem.*, 1995, **34**, 2382.
35 A. Neves, M. A. Brito, I. Vencato, V. Drago, K. Griesar and W. Haase, *Inorg. Chem.*, 1996, **35**, 2360.

36 M. Suzuki, S. Fujinami, T. Hibino, H. Hori, Y. Maeda, A. Uehara and M. Suzukui, *Inorg. Chim. Acta*, 1998, **283**, 124.
37 A. Horn, Jr., A. Neves, I. Vencato, V. Drago, C. Zucco, R. Werner and W. Haase, *J. Braz. Chem. Soc.*, 2000, **11**, 1; A. Horn, Jr., A. Neves, I. Vencato, V. Drago, C. Zucco, R. Werner and W. Haase, *J. Braz. Chem. Soc.*, 2000, **11**, 7.
38 B. Krebs, K. Schepers, B. Bremer, G. Henkel, E. Althaus, W. Müller-Warmuth, K. Griesar and W. Haase, *Inorg. Chem.*, 1994, **33**, 1907.
39 M. A. Brito, A. Neves, I. Vencato, C. Zucco, V. Drago, K. Griesar and W. Haase, *J. Braz. Chem. Soc.*, 1997, **8**, 5; M. A. Brito, A. Neves, I. Vencato, C. Zucco, V. Drago, K. Griesar and W. Haase, *J. Braz. Chem. Soc.*, 1997, **8**, 443.
40 J. Wang, M. S. Mashuta, Z. Sun, J. F. Richardson, D. N. Hendrickson and R. M. Buchanan, *Inorg. Chem.*, 1996, **35**, 6642.
41 S. M. Gorun and S. J. Lippard, *Inorg. Chem.*, 1991, **30**, 1625.
42 D. P. E. Dickson and F. J. Berry, in *Mössbauer Spectroscopy*, 1st edn., Cambridge University Press, Cambridge, 1986, ch. 3, pp. 121–124.
43 E. W. Ainscough, A. M. Brodie, J. E. Plowman, K. L. Brown, A. W. Addison and A. R. Gainsford, *Inorg. Chem.*, 1980, **19**, 3655.